Electronic Supplementary Material (ESI) for Lab on a Chip.

Supplementary Information

Generation of dynamic vortices in a microfluidic system incorporating stenosis barrier by tube oscillation

Peter Thurgood [1,†], Chanly Chheang [2], Scott Needham [3], Elena Pirogova [1], Karlheinz Peter [4, 5], Sara Baratchi [2, *, †], Khashayar Khoshmanesh [1,*, †]

[1] School of Engineering, RMIT University, Melbourne, Victoria, Australia

[2] School of Health & Biomedical Sciences, RMIT University, Bundoora, Victoria, Australia

† Corresponding authors:

Peter Thurgood: peter.thurgood@rmit.edu.au

Khashayar Khoshmanesh: khashayar.khoshmanesh@rmit.edu.au

Sara Baratchi: sara.baratchi@rmit.edu.au

* There authors contributed equally to this work.

Keywords: microfluidics, vortex generation, dynamic flows, inertial

Supplementary Information 1: Geometrical details of the microfluidic structure

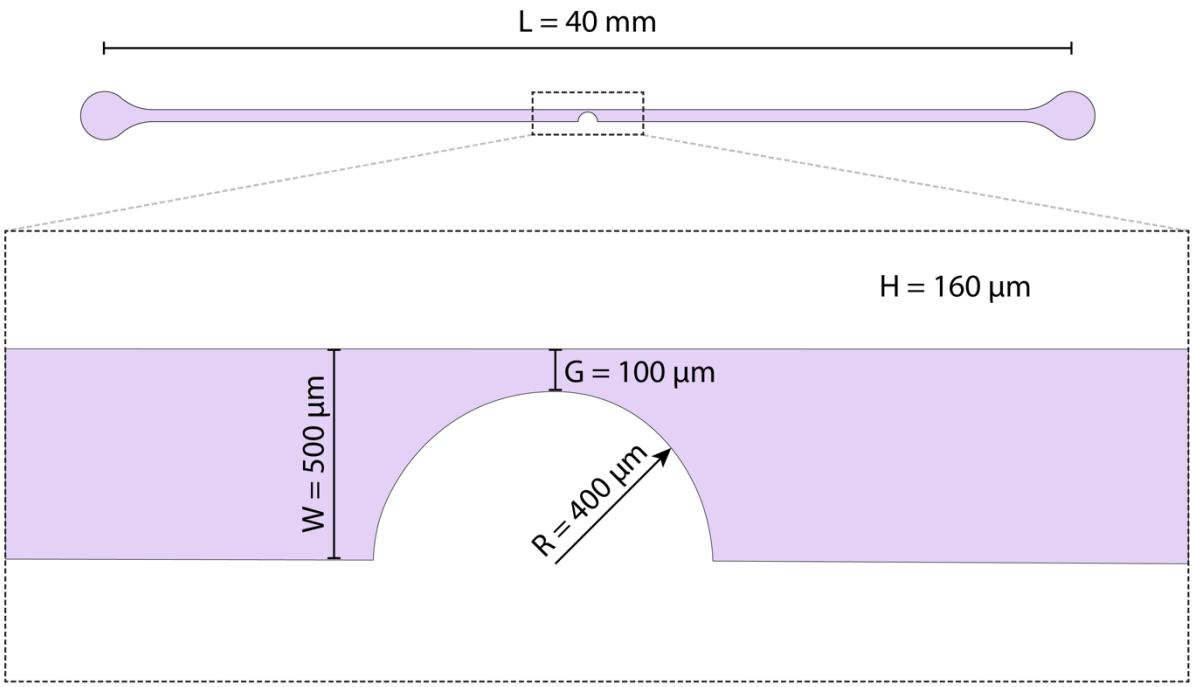

Figure S1. Schematics of a microfluidic channel incorporating a circular stenosis utilised for the generation of dynamic vortices.

Supplementary Information 2: Characterisation of the audio speaker

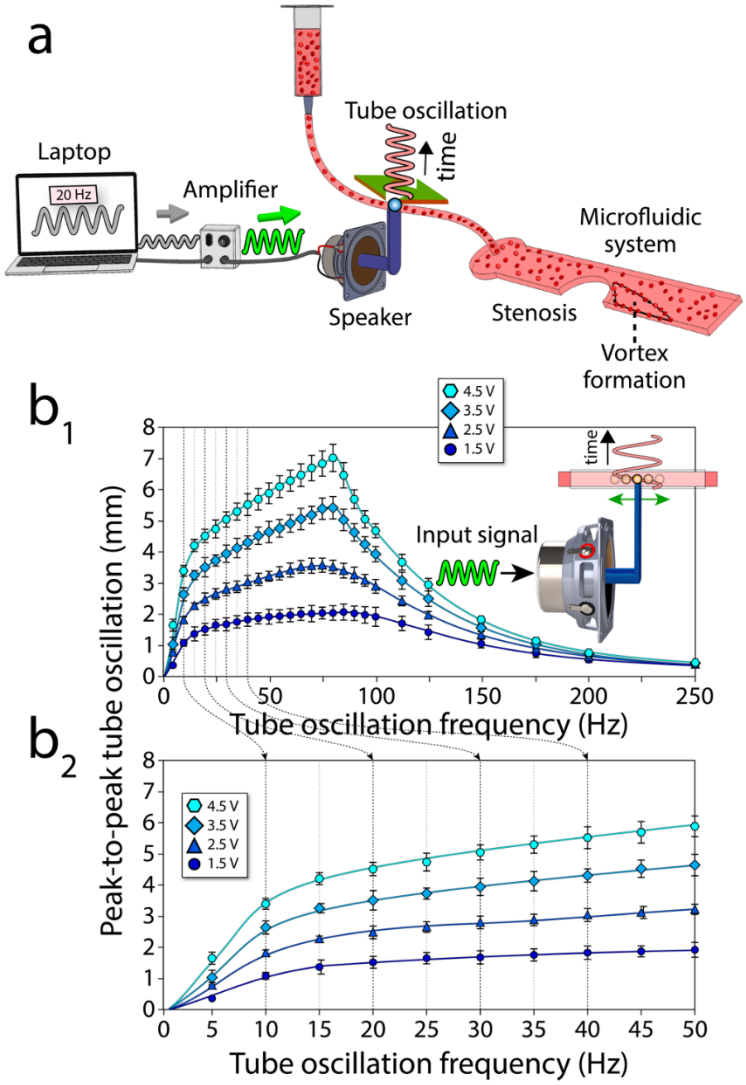

Figure S2. Characterisation of the audio speaker: **(a)** Schematics of the system. **(b)** Variations of tube oscillation amplitude against tube oscillation frequency at various voltages applied to the speaker.

Supplementary Information 3: Characterisation of tube oscillation at different points of the inlet tube

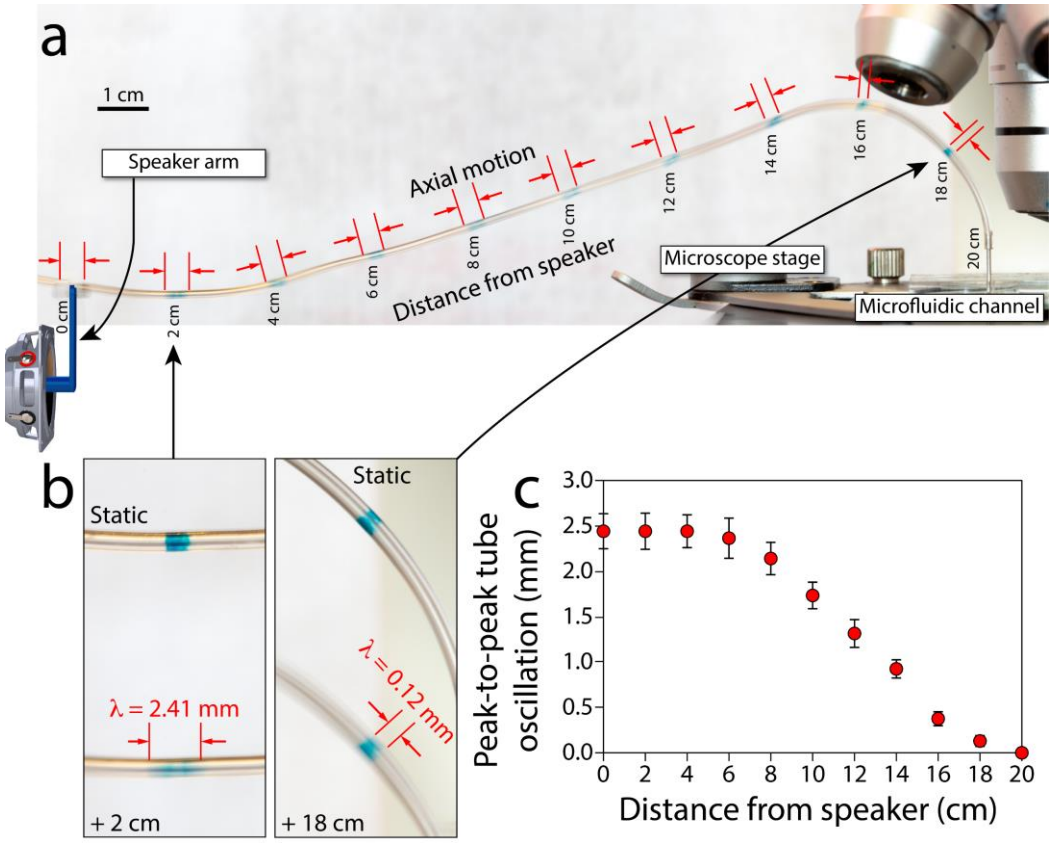

Figure S3. Analysing the axial oscillation of the inlet tube obtained by a 1 s exposure using a Canon 6D camera coupled with an EF 100 mm f/2.8 macro lens: **(a)** Amplitude of axial oscillation at different points of the inlet tube. Blue strips were drawn using a marker at 2 cm intervals to track the tube oscillation. **(b)** Close-up images at the points positioned 2 cm and 18 cm away from the speaker arm. **(c)** Variations of the tube axial oscillation amplitude against the tangential distance from the speaker arm. Error bars correspond to average ± standard deviation obtained in three sets of independent experiments.

Supplementary Information 4: Assessing the biocompatibility of tube oscillation

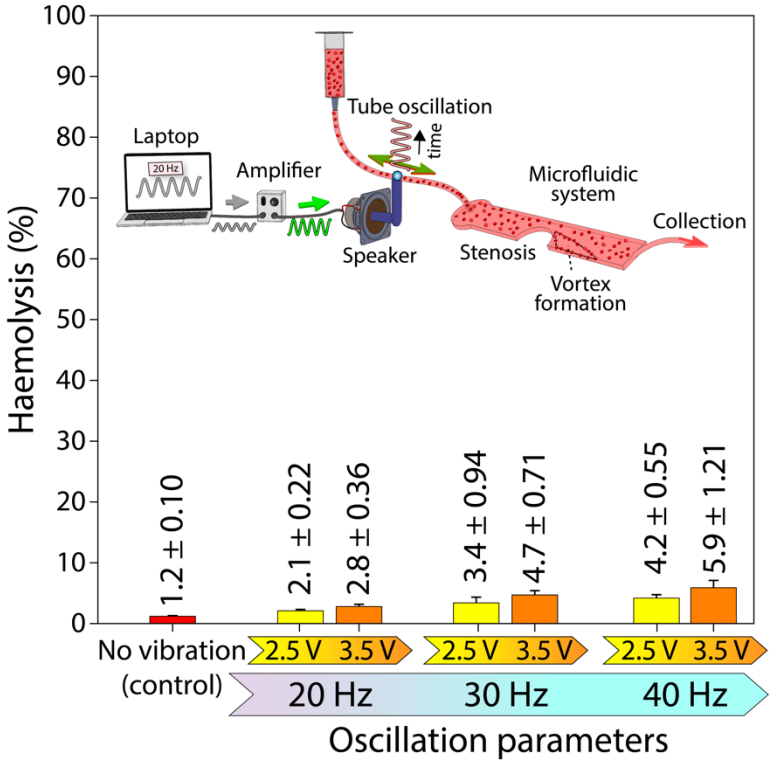

Figure S4. Analysis of the haemolysis of blood samples following tube oscillation at various oscillation frequencies and voltages.

Supplementary Information 5: Calculation of the equivalent velocity of oscillating flow

The dynamic velocity of the fluid within the oscillating tube ($U_{dynamic}$) can be obtained by providing a balance between the dynamic pressure induced by tube oscillation and the viscous pressure drop along the tube and the microfluidic channel:

$$\Delta P_{oscillation} = \Delta P_{viscous-tube} + \Delta P_{viscous-channel} \quad (1)$$

These three pressure terms can be defined as below:

$$\Delta P_{oscillation} = 0.5\, \rho_{fluid} (\lambda_{tube}\, \omega_{tube})^2 \left(L_{oscillating} / L_{tube} \right) sin(\omega_{tube}\, t) \quad (2)$$

$$\Delta P_{viscous-tube} = 128\, \mu_{fluid}\, Q_{dynamic}\, L_{tube} / \pi D_{tube}^4 \quad (3)$$

$$\Delta P_{viscous-channel} = a_{ch}\, \mu_{fluid}\, Q_{dynamic}\, L_{ch} / W_{ch} H_{ch}^3 \quad (4)$$

in which, ρ_{fluid} and μ_{fluid} are the density and viscosity of the fluid, λ_{tube} and ω_{tube} are the amplitude and frequency of tube oscillation, respectively, $Q_{dynamic}$ is the dynamic flow rate induced by tube oscillation, L_{tube} and D_{tube} are the length and internal diameter of the oscillating tube, respectively, $L_{oscillating}$ is the length of the tube, which is oscillating almost at the same amplitude of the audio speaker diaphragm, L_{ch}, W_{ch} and H_{ch} are the length, width, and height of the microfluidic channel, respectively, a_{ch} is the aspect ratio coefficient of the channel, which is defined as $a_{ch} = 12/[1 - (192\, H_{ch}/\pi^5 W_{ch}) \tanh (\pi\, W_{ch}/2\, H_{ch})]$.

Rearranging of the above equations, the dynamic velocity of the oscillating tube is obtained, as below:

$$Q_{dynamic}(t) = \frac{0.5\, \rho_{fluid} (\lambda_{tube}\, \omega_{tube})^2\, L_{oscillating} / L_{tube}\, sin(\omega_{tube}\, t)}{128\, \mu_{fluid}\, L_{tube} / \pi D_{tube}^2 + a_{ch}\, \mu_{fluid}\, L_{ch} / W_{ch} H_{ch}^3} \quad (5)$$

Accordingly, the dynamic velocity of the fluid within the oscillating tube is obtained, as below:

$$U_{dynamic}(t) = \frac{4\, Q_{dynamic}(t)}{\pi D_{tube}^2} \quad (6)$$

Supplementary Information 6: Vortex generation downstream the stenosis under static flow conditions

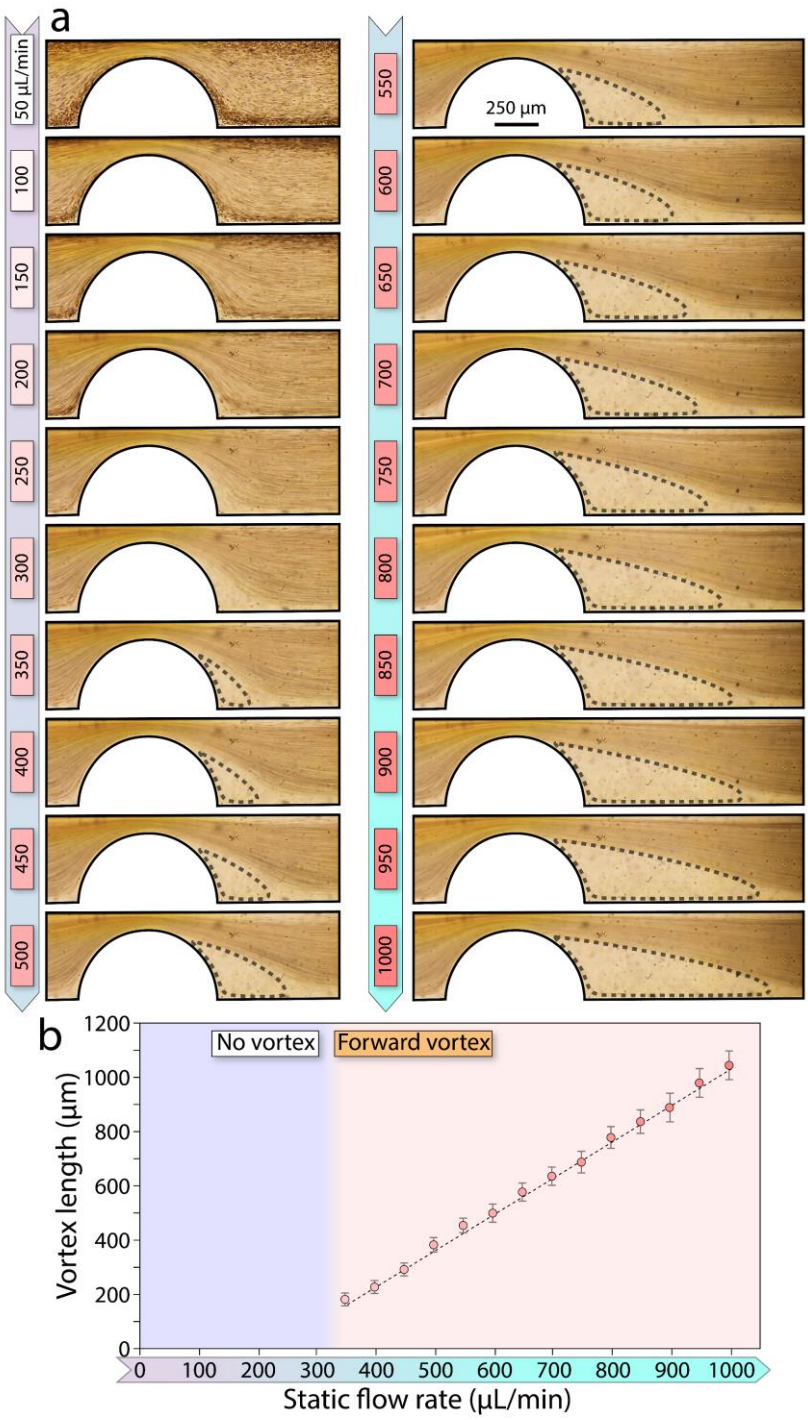

Figure S5. Vortex formation downstream of a stenosis at static flow rates without tube oscillation: **(a)** The formation of a forward vortex in diluted blood at flow rates higher than 350 µL/min captured by high-speed imaging. **(b)** Variations of vortex length against static flow rate. Error bars correspond to average ± standard deviation obtained from three sets of independent experiments.

Supplementary Information 7: Evolution of dynamic vortices obtained by numerical simulations

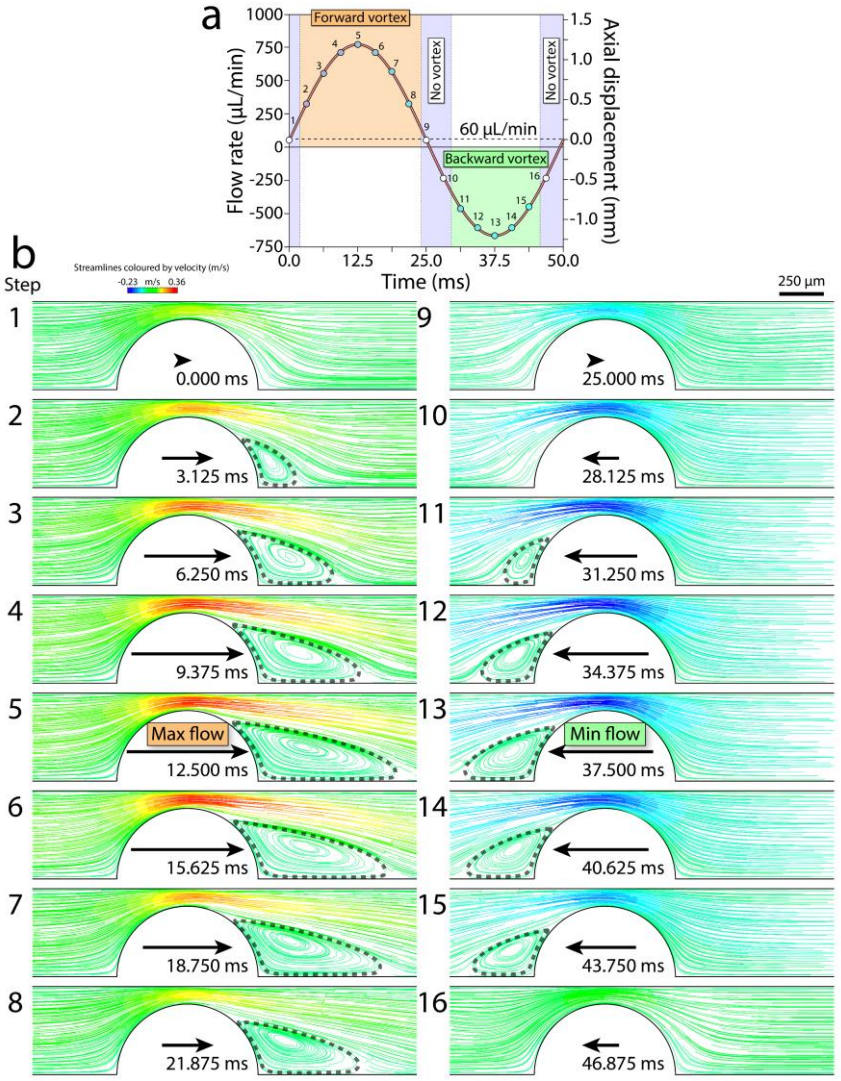

Figure S6. Numerical simulations showing the evolution of dynamic vortices: **(a)** Dynamic flow rates induced by tube oscillation in the microfluidic channel. **(b)** The evolution of backward and forward vortices over a single tube oscillation cycle obtained by numerical simulations.

Supplementary Information 8: Variations of vortex extent and area over one cycle

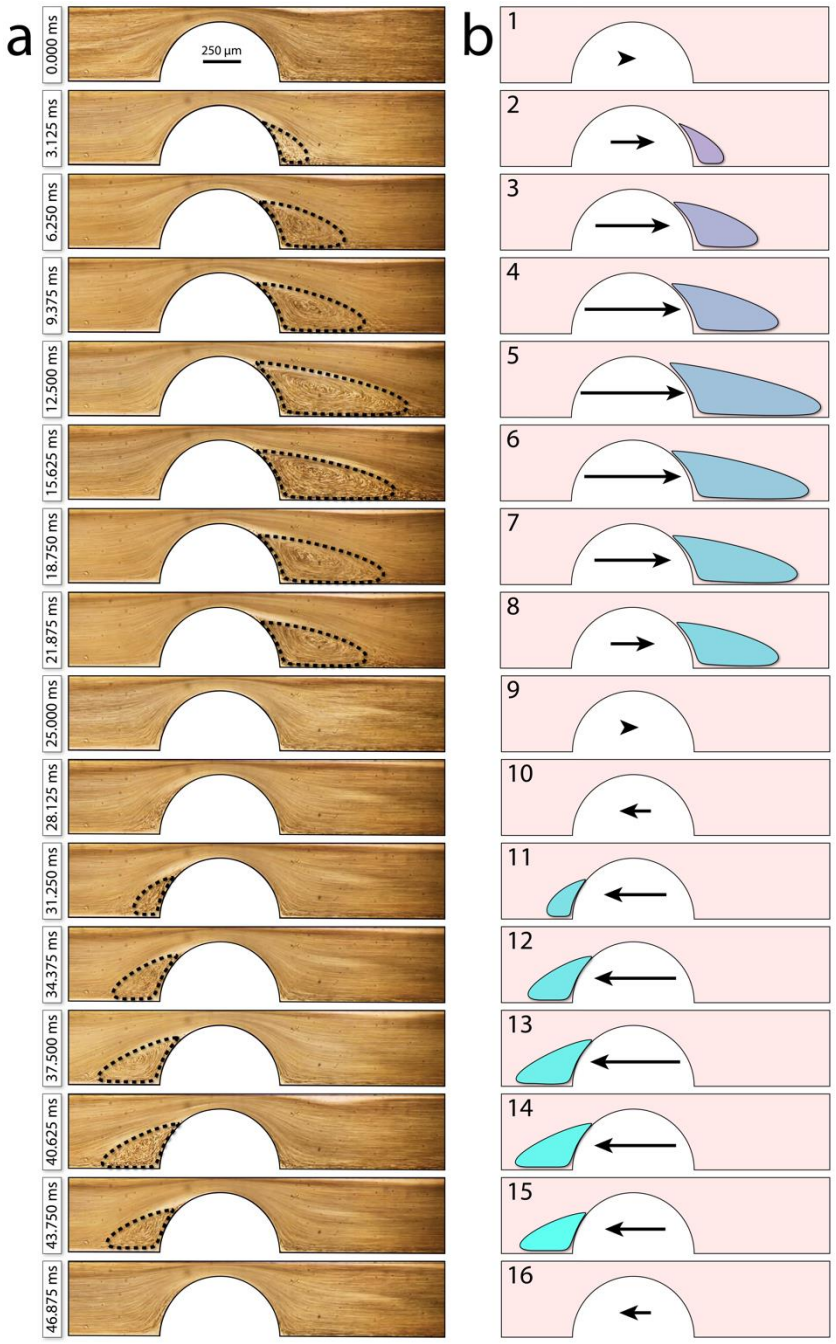

Figure S7-i. The evolution of backward and forward vortices over time: **(a)** Vortex formation in diluted blood at 2.5 V and 20 Hz over one cycle obtained by high-speed imaging. **(b)** Schematics showing the extent of backward and forward vortices.

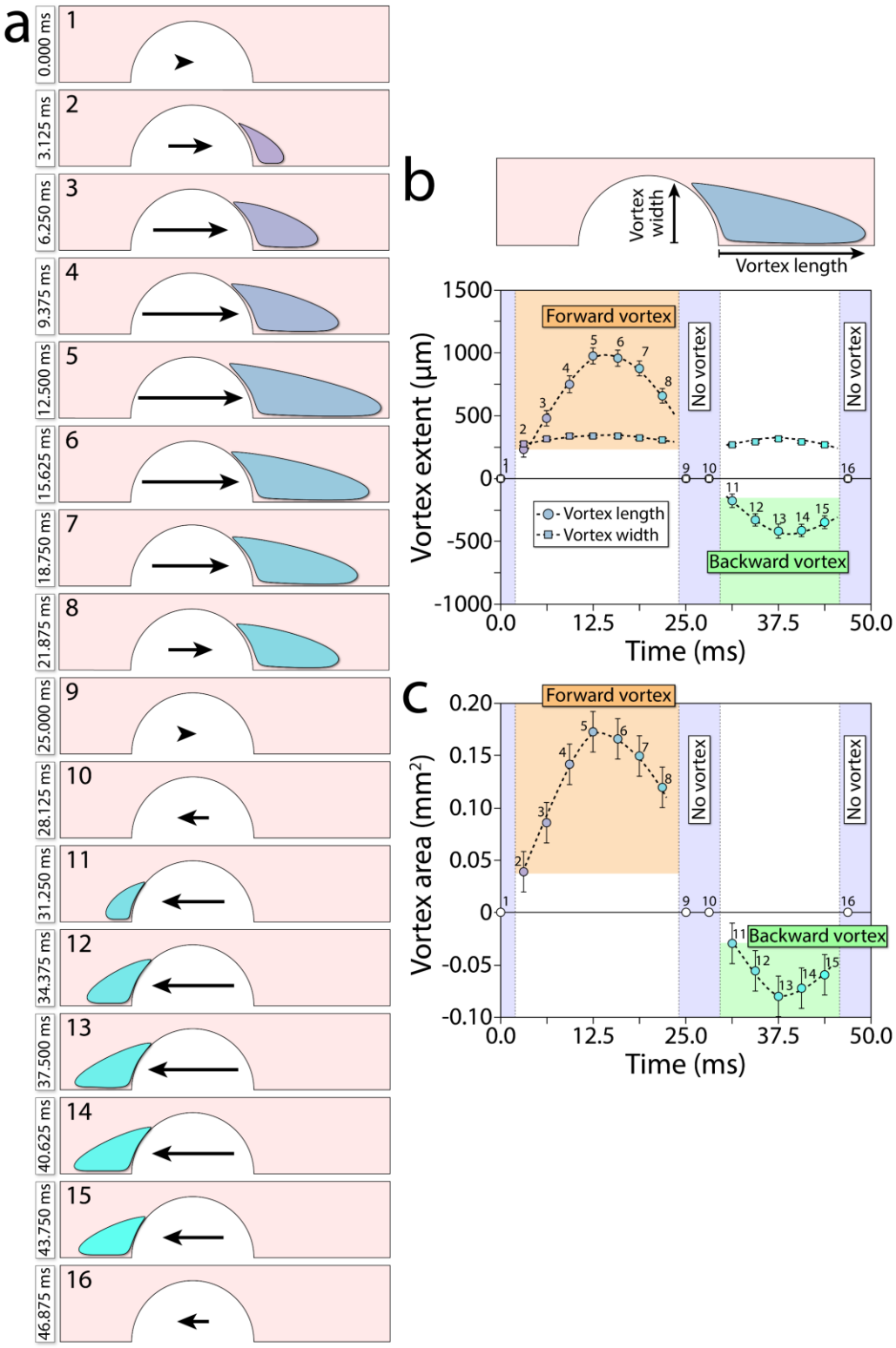

Figure S7-ii. The vortex evolution over time: **(a)** Schematics showing the extent of backward and forward vortices at 2.5 V and 20 Hz over one cycle. **(b)** Variations of vortex extent (length and width) over time. **(d)** Variations of vortex area over time obtained by ImageJ. Error bars corresponds to average ± standard deviation obtained in three sets of independent experiments.

Supplementary Information 9: Discontinuous generation of dynamic vortices

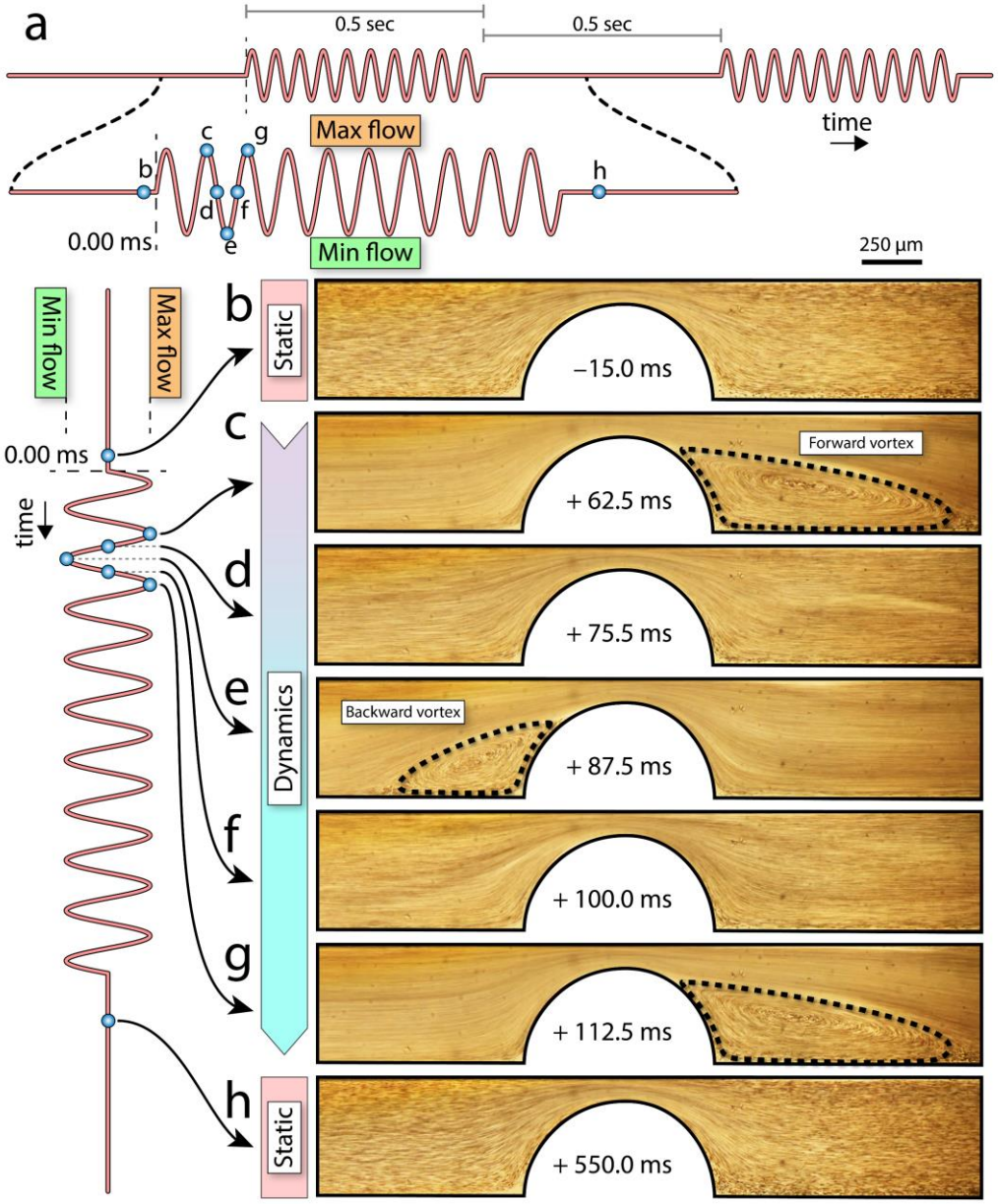

Figure S8. Discontinuous generation of dynamic vortices: **(a)** A discontinuous 20 Hz, 2.5 V signal with 0.5 sec pulses and 0.5 sec gaps to activate the audio speaker. **(b)** No-vortex mode. **(c-g)** Dynamic vortex generation caused by tube oscillation. **(h)** Return to no-vortex mode.

Supplementary Information 10: Dynamic vortex generation at various frequencies obtained by numerical simulations

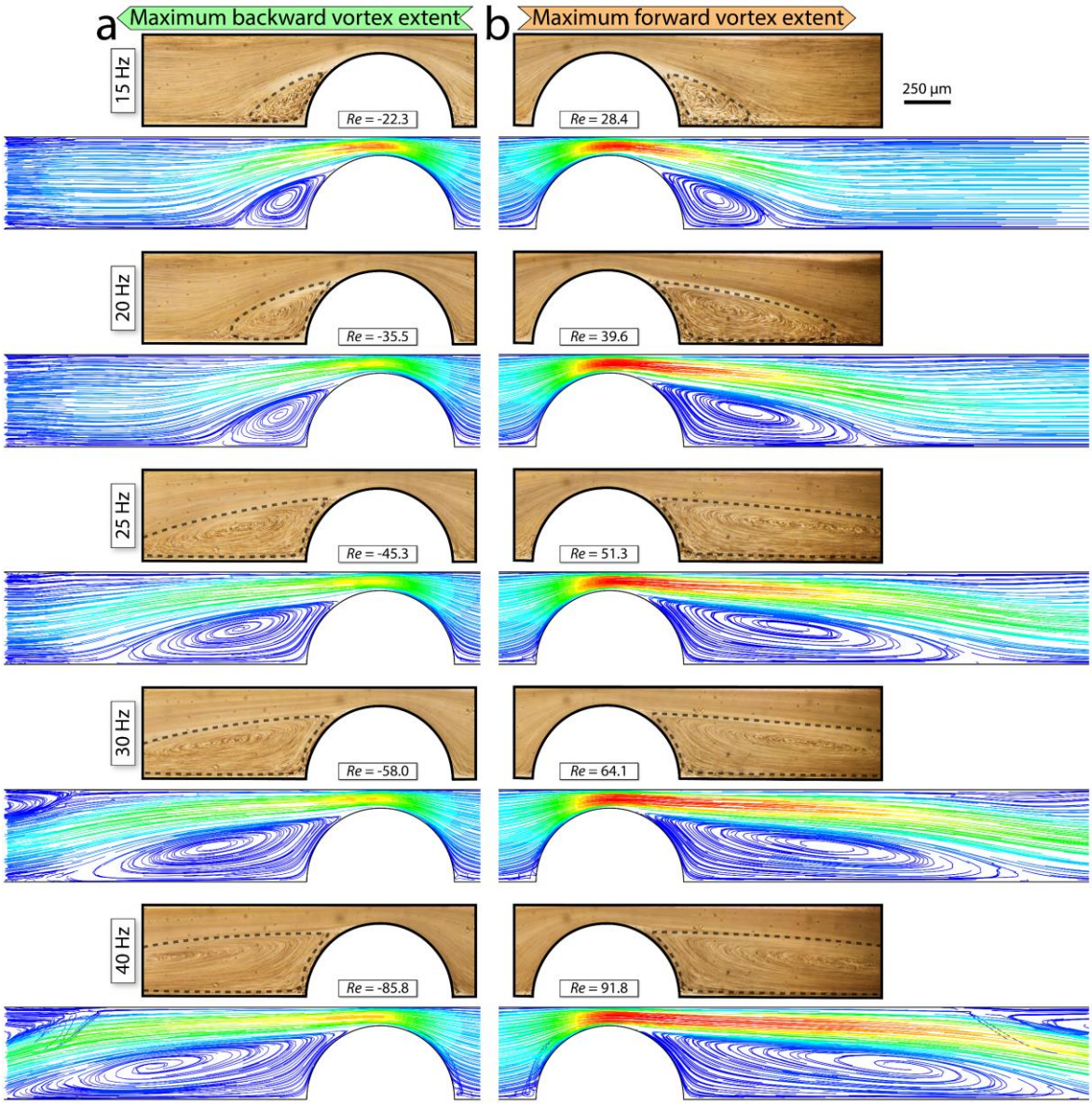

Figure S9. Numerical simulations to investigate dynamic vortex generation at oscillation frequencies ranging from 15 to 40 Hz at 2.5 V: **(a-b)** The extent of backward and forward vortices obtained by numerical simulations which closely match experimental results.

Supplementary Information 11: Generation of a secondary vortex at higher frequencies

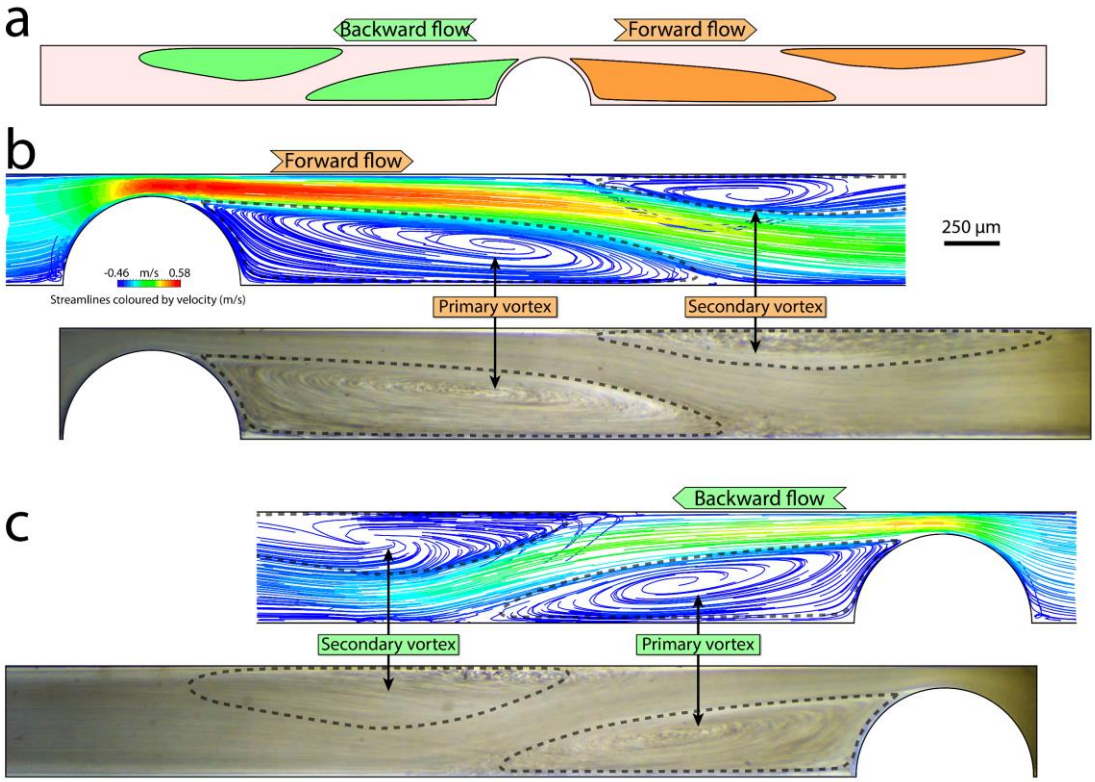

Figure S10. Generation of a secondary vortex at high frequencies: **(a)** Schematics showing the location of primary and secondary backward and forward vortices. **(b)** Simulation and experimental results showing the formation of primary and secondary forward vortices. **(c)** Simulation and experimental results showing the formation of primary and secondary backward vortices. Results are obtained by setting the frequency of tube oscillation to 35 Hz and the voltage of the speaker to 2.5 V.

Supplementary Information 12: Variations of vortex width at different tube oscillation frequencies

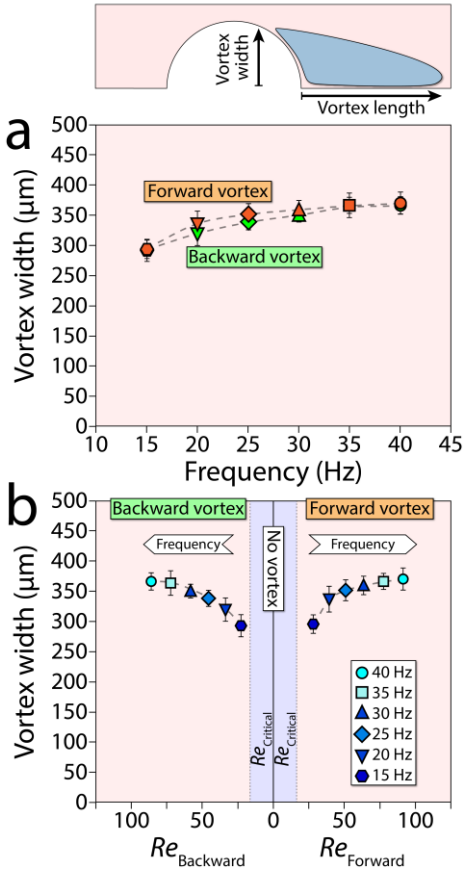

Figure S11. Variations of vortex width (progression along the width of the channel) at different oscillation frequencies: **(a)** Variations of vortex width against frequency. **(b)** Variations of vortex width against the Reynolds number of oscillating flow. Error bars corresponds to average ± standard deviation obtained in three sets of independent experiments.

Supplementary Information 13: Variations of vortex width at different voltages

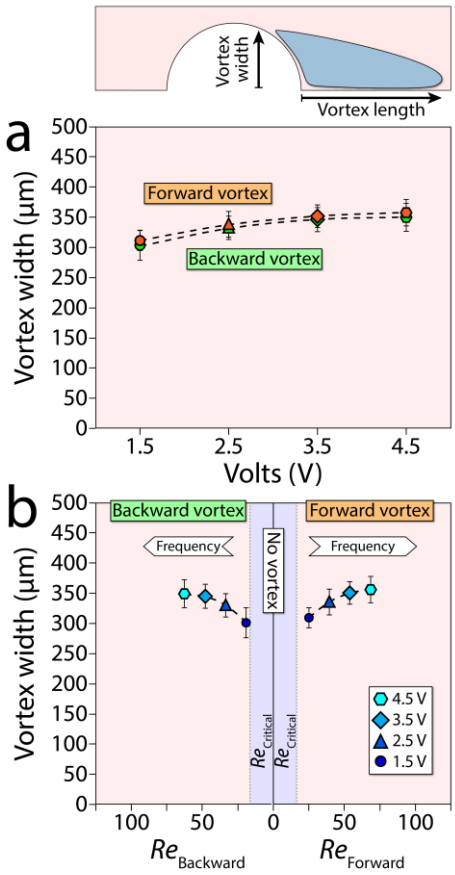

Figure S12. Variations of vortex width (progression along the width of the channel) at different voltages applied to the audio speaker: **(a)** Variations of vortex width against voltage. **(b)** Variations of vortex width against the Reynolds number of oscillating flow. Error bars corresponds to average ± standard deviation obtained in three sets of independent experiments.

Supplementary Information 14: Dynamic vortex generation at 30 Hz at various voltages

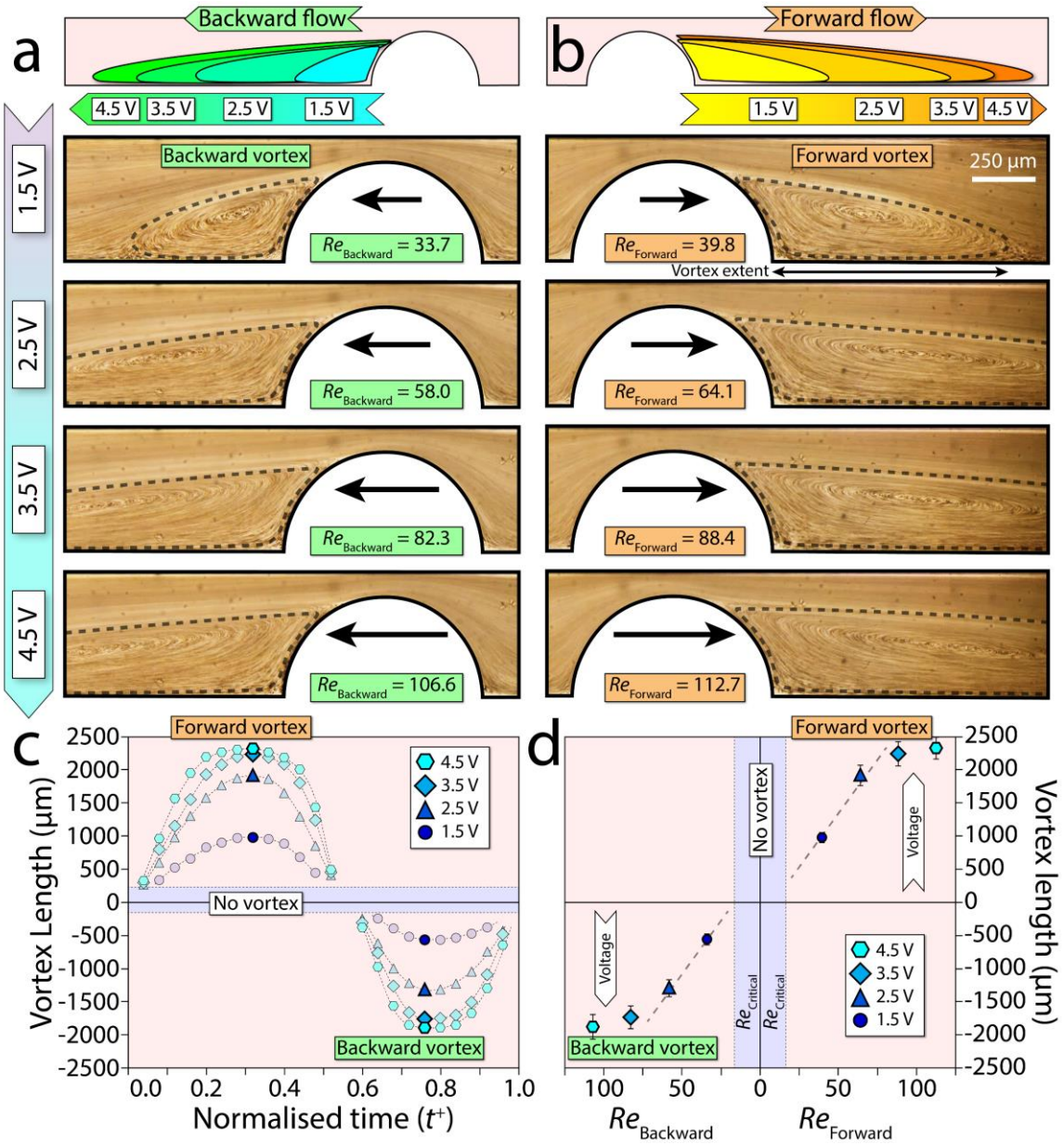

Figure S13. The effect of input voltage on the generation of dynamic vortices across a microfluidic stenosis: **(a-b)** The extent of backward and forward vortices at 30 Hz and at voltages ranging from 1.5 V to 4.5 V. **(c)** Variations of vortex length over one oscillation cycle at different voltages at 30 Hz. **(d)** Variations of vortex length against the Reynolds number of oscillating flow at different voltages at 30 Hz.

Supplementary Information 15: Dynamic vortex generation at higher flow rates obtained by numerical simulations

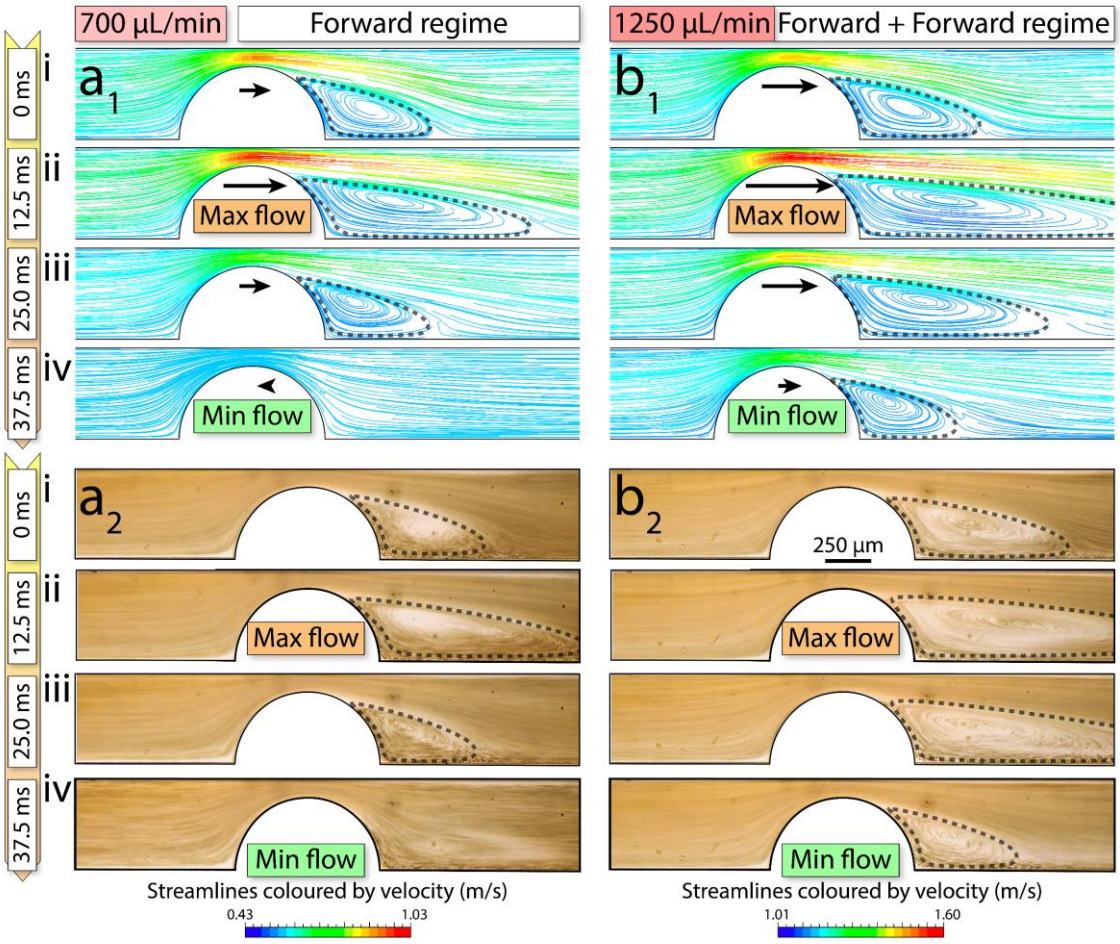

Figure S14. Analysing the dynamics of vortices at high flow rates using numerical simulations: **(a)** A flow rate of 700 µL/min inducing the forward vortex regime. **(b)** 1250 µL/min inducing forward-forward vortex regime.

Supplementary Information 16: Analysis of flow-induced shear rate induced at the stenosis

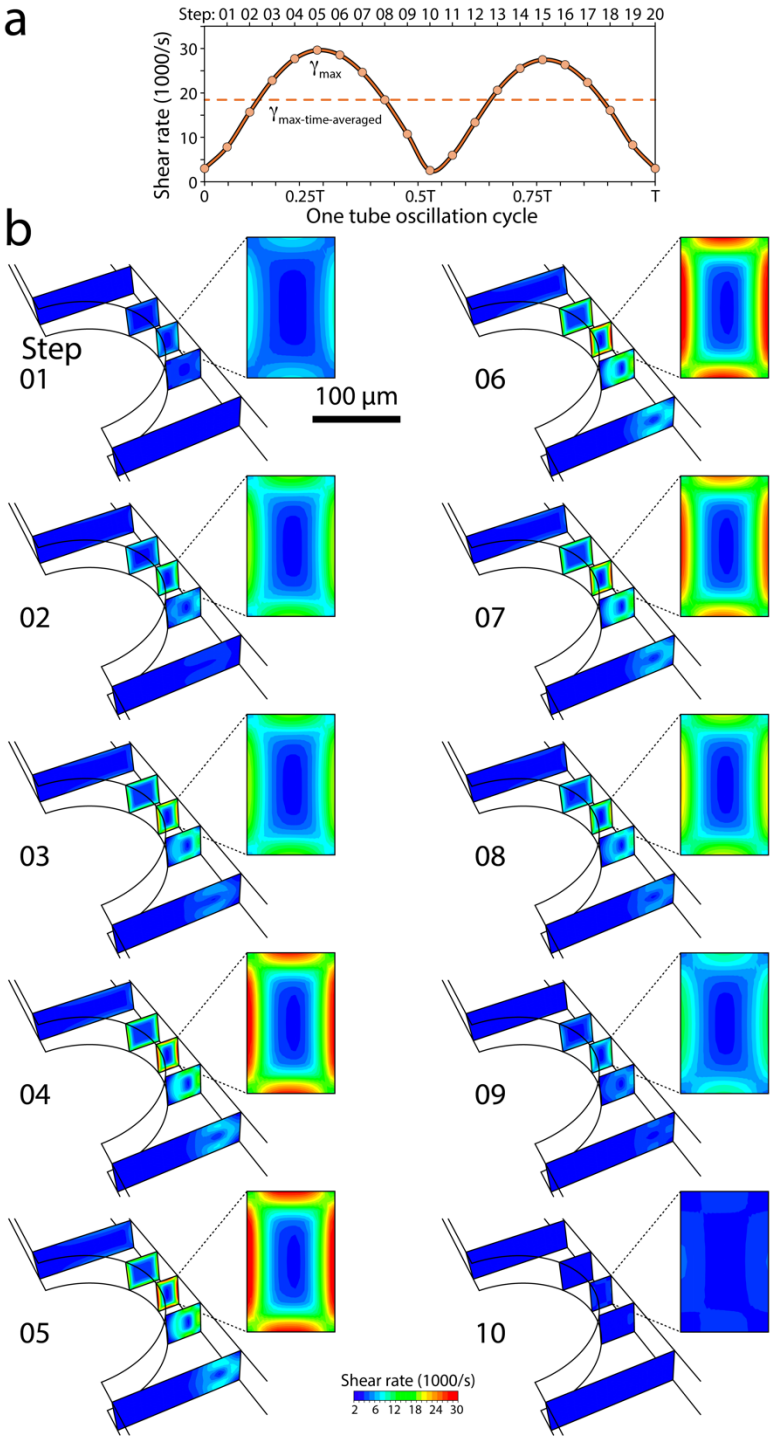

→ continued on the next page

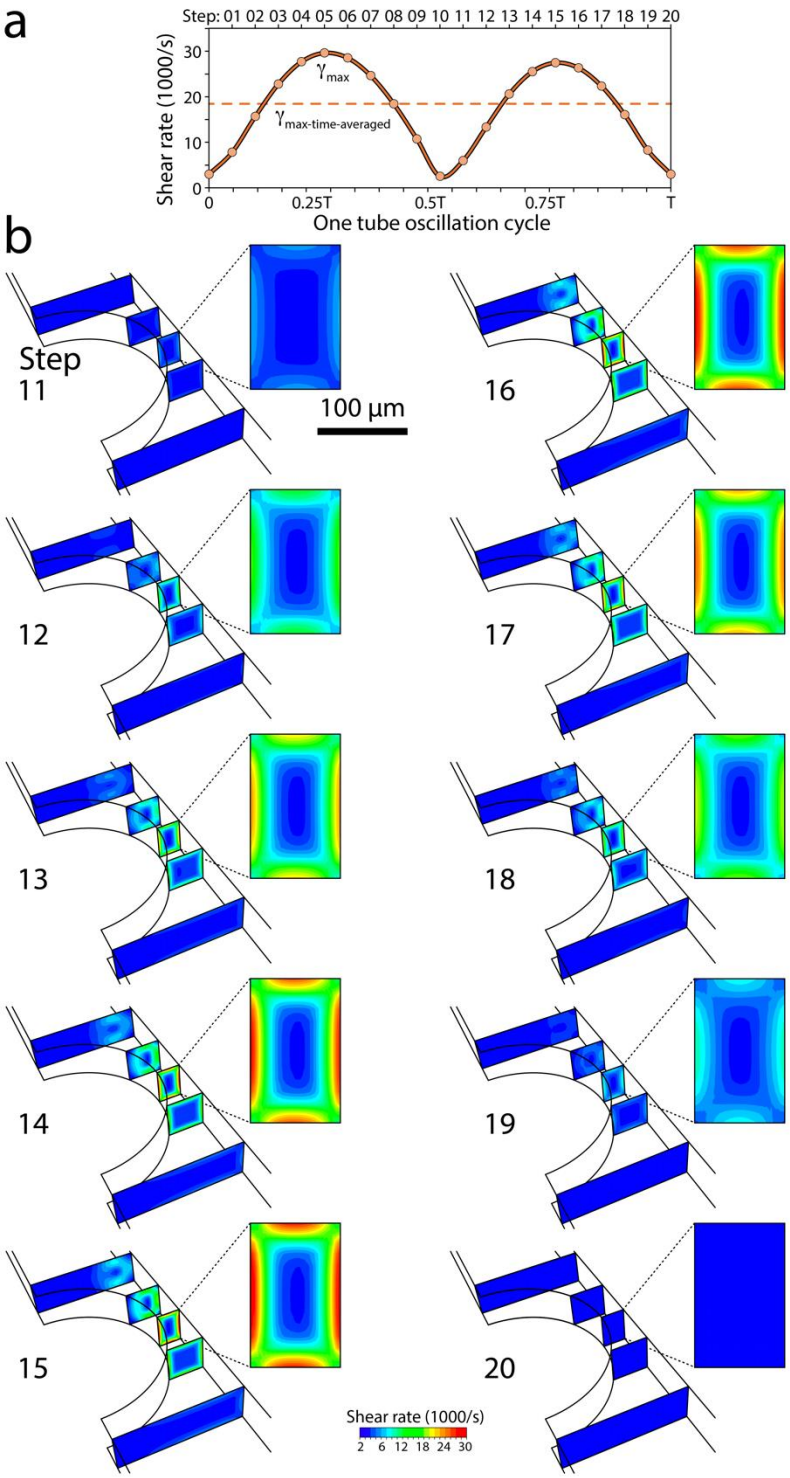

Figure S15. Variations of shear rate throughout a tube oscillation cycle obtained by numerical simulations. **(a)** Variations of maximum shear rate at the apex of stenosis within one cycle of tube oscillation. **(b)** Shear rate contours at the cross-section of the stenosed microfluidic channel obtained. Results are obtained by setting the tube oscillation frequency to 30 Hz and the speaker voltage to 3.5 V.